University of Dundee

Slow-Binding Inhibition of Mycobacterium tuberculosis Shikimate Kinase by Manzamine Alkaloids

Simithy, Johayra; Fuanta, Ngolui Rene; Alturki, Mansour; Hobrath, Judith V.; Wahba, Amir E.; Pina, Ivett

Supporting information for:

Slow-binding inhibition of *Mycobacterium tuberculosis* shikimate kinase by manzamine alkaloids

Johayra Simithy[a,g], Ngolui Rene Fuanta[b,g], Mansour Alturki[a], Judith V. Hobrath[c], Amir E. Wahba[d],

Ivett Pina[e], Jnanendra Rath[f], Mark T. Hamann[e], Jack DeRuiter[a], Douglas C. Goodwin[b], Angela I.

Calderón[a]*

[a]Department of Drug Discovery and Development, Harrison School of Pharmacy, 4306 Walker Building, Auburn University, Auburn, AL 36849, USA.

[b]Department of Chemistry and Biochemistry, 179 Chemistry Building, Auburn University, Auburn, AL 36849, USA.

[c]Department of Chemistry, University of Alabama at Birmingham, Birmingham, AL 35294, USA; current affiliation: Drug Discovery Unit, College of Life Sciences, University of Dundee, Dundee DD1 5EH, United Kingdom.

[d]Chemistry Department, Faculty of Science, Damietta University, Egypt.

[e]Departments of Drug Discovery & Biomedical Sciences and Public Health, Colleges of Pharmacy and Medicine 70 President Street, MSP 139, Charleston, SC 29425, USA.

[f]Department of Botany, Visva-Bharati University, Santiniketan, West Bengal, 731235, India.

[g]These authors contributed equally to the work described.

Supporting Information Table of Contents

Table S1. Marine compounds evaluated in the current study, including molecular weight and molecular formula.

Compound	Molecular weight (Da)	Molecular formula
3-bromotyramine	216.08	$C_8H_{10}BrNO$
4-hydroxybenzaldehyde	122.12	$C_7H_6O_2$
6-cyclohexamidemanzamine A	673.92	$C_{43}H_{55}N_5O_2$
6-deoxy-manzamine X	564.76	$C_{36}H_{44}N_4O_2$
6-nitroharmane	227.07	$C_{12}H_9N_3O_2$
8-isopropyl-manzamine A	606.39	$C_{39}H_{50}N_4O_2$
8-OH-manzamine	564.35	$C_{36}H_{44}N_4O_2$
Aaptamine	228.25	$C_{13}H_{12}N_2O_2$
Aplysinopsin	254.29	$C_{14}H_{14}N_4O$
Curcudiol	236.18	$C_{15}H_{24}O_2$
Cyanthiwigin C	288.47	$C_{20}H_{32}O$
Elysia_910	909.50	Unknown
Hawaiimycin B	344.20	$C_{48}H_{82}O_{18}$
Hawaiimycin C	960.57	$C_{49}H_{84}O_{18}$
Ilimaquinone	344.20	$C_{21}H_{28}O_4$
Indole-3-carboxaldehyde	145.16	C_9H_7NO
Ircinal A	410.29	$C_{26}H_{38}N_2O_2$
Ircinol A	412.60	$C_{26}H_{40}N_2O_2$
Isoaaptamine	228.25	$C_{13}H_{12}N_2O_2$
Kahalalide F	1476.93	$C_{75}H_{124}N_{14}O_{16}$
Manzamine A	548.35	$C_{22}H_{24}Br_2N_{10}O_2$
Manzamine D	552.79	$C_{36}H_{48}N_4O$
Manzamine E	564.76	$C_{36}H_{48}N_4O$
Manzamine F	580.00	$C_{36}H_{44}N_4O_3$
Sceptrin	620.29	$C_{22}H_{24}Br_2N_{10}O_2$
Theonellapeptilide 1d	1404.00	Unknown

Purity of compounds (1 - 6) by ¹H NMR, LC-MS and MS/MS.
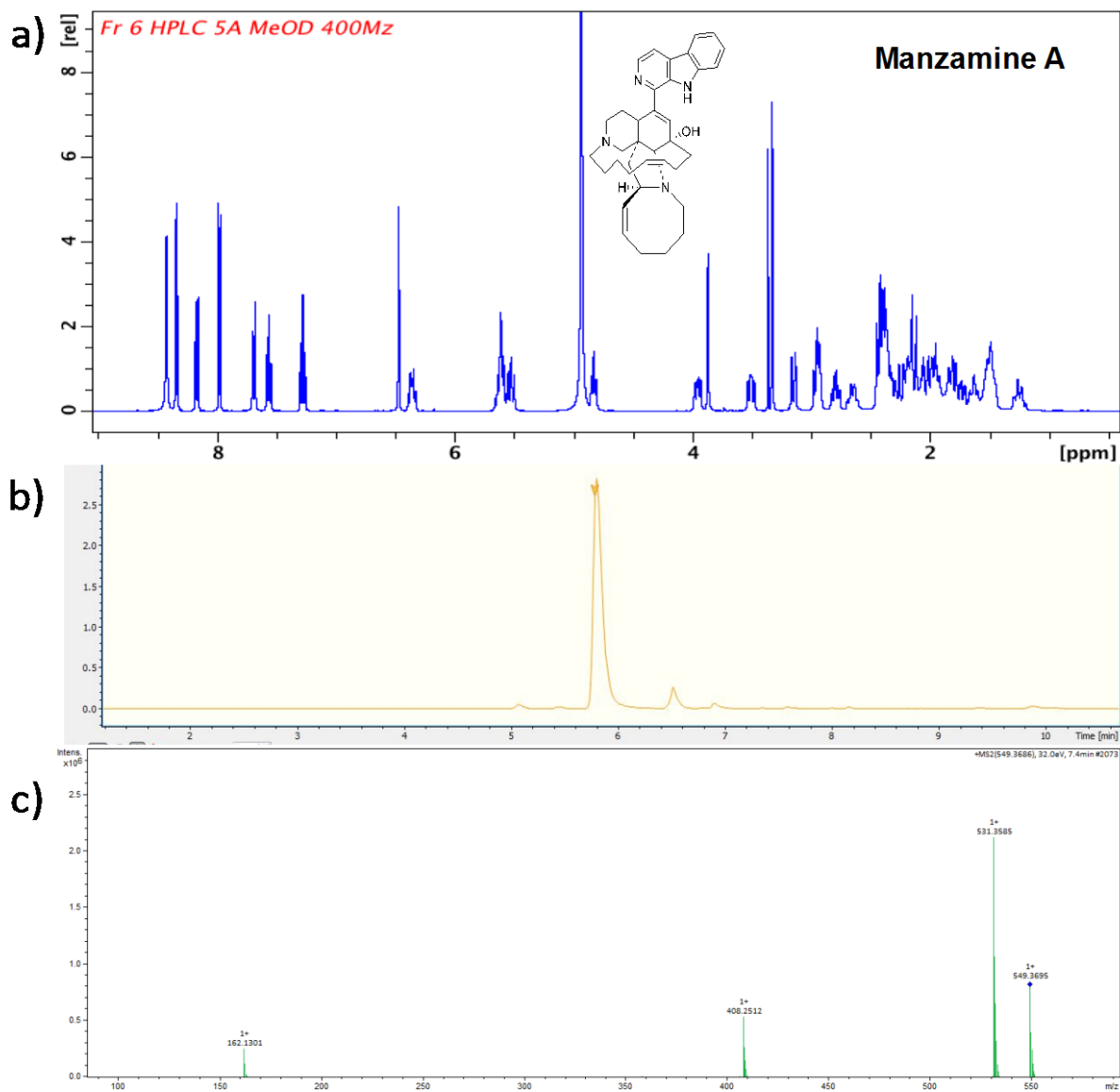
Figure S1. a) ¹H NMR spectrum (400 MHz, pyridine-d5), b) LCMS and c) MS/MS of manzamine A (**1**).
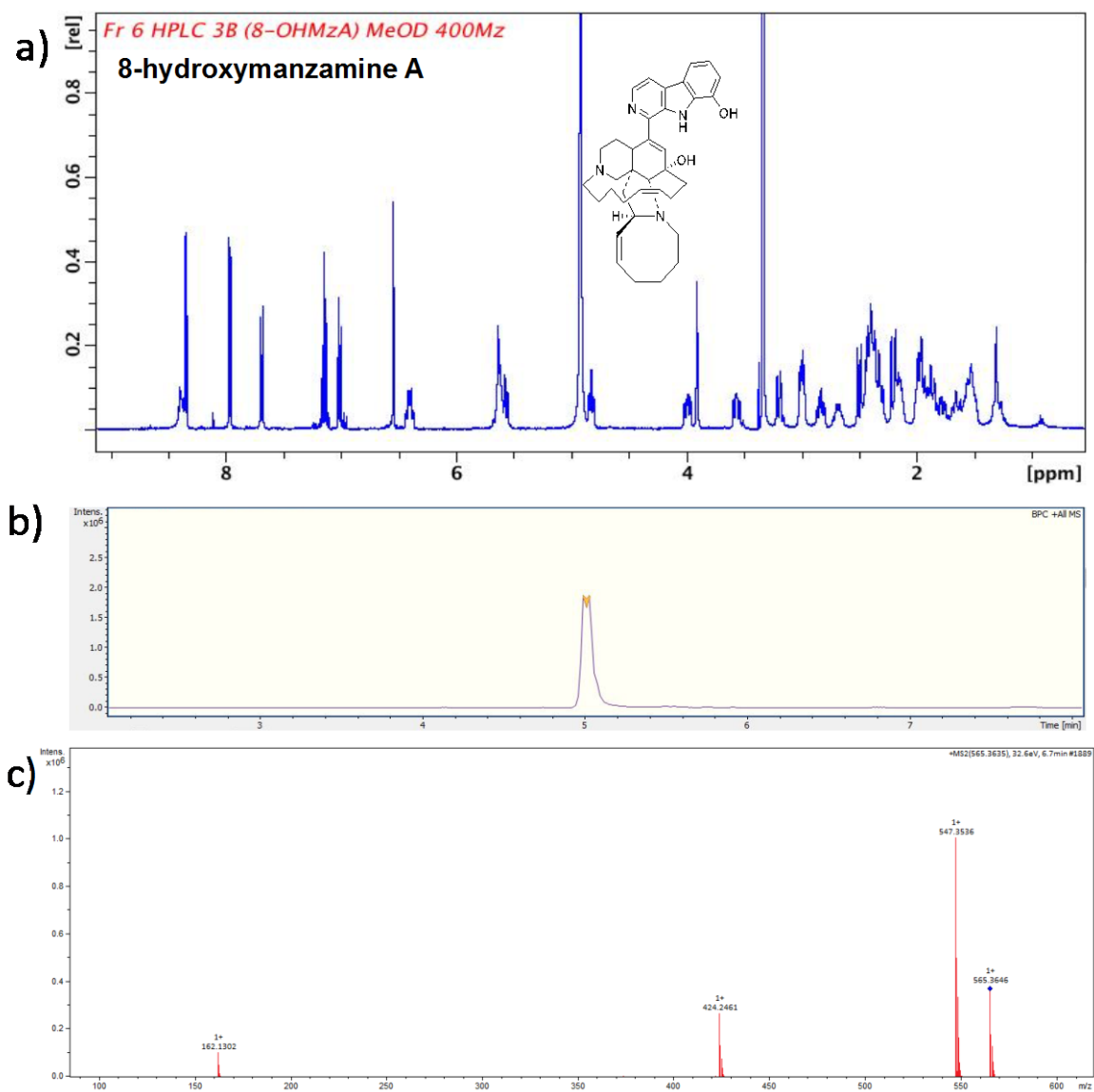
Figure S2. A) ^{1}H NMR spectrum (400 MHz, pyridine-d5) b), LCMS and c) MS/MS of 8 hydroxymanzamine A (**2**).
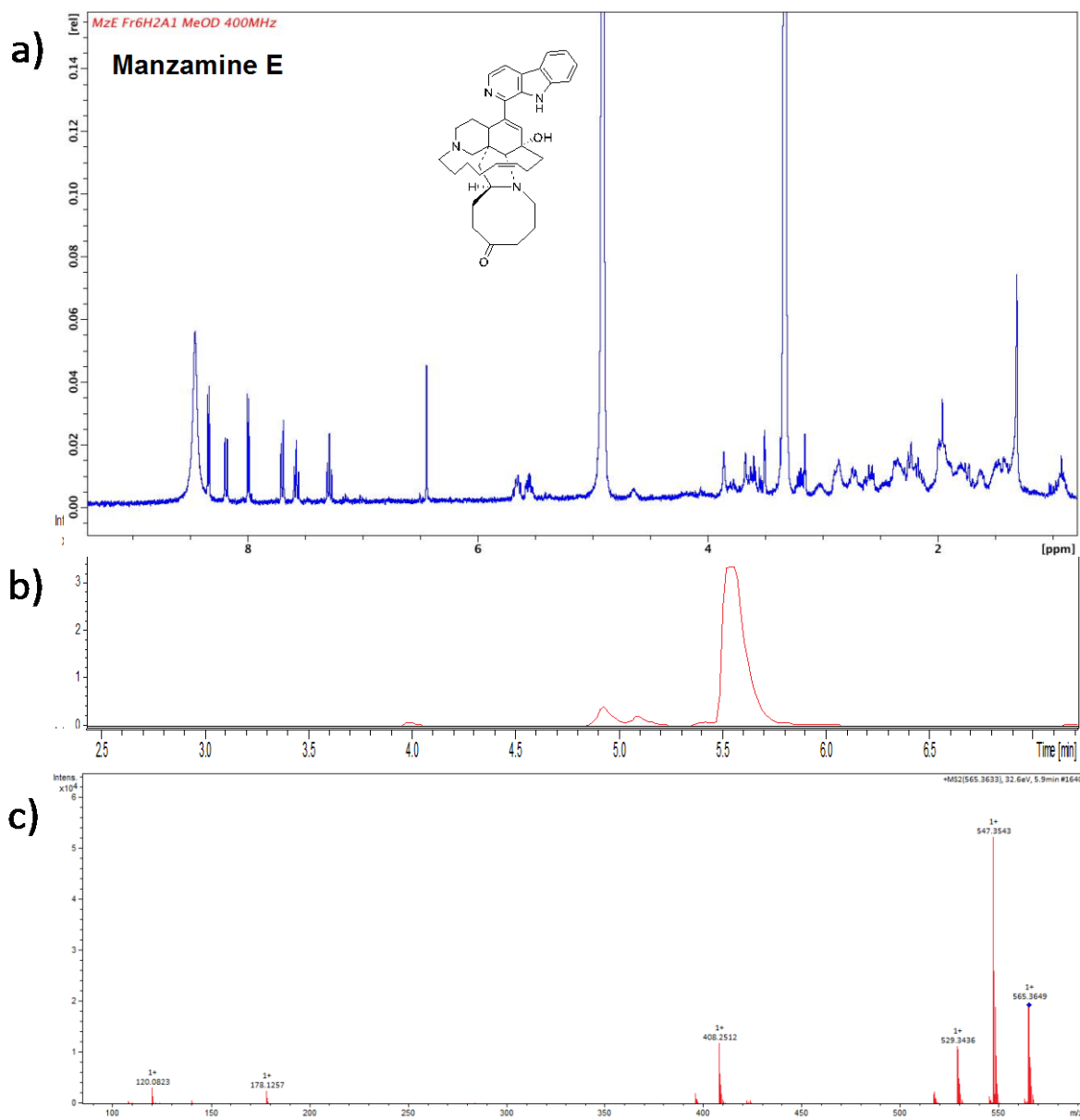
Figure S3. a) ^{1}H NMR spectrum (400 MHz, Methanol-d4), b) LCMS and c) MS/MS of manzamine E (**3**).
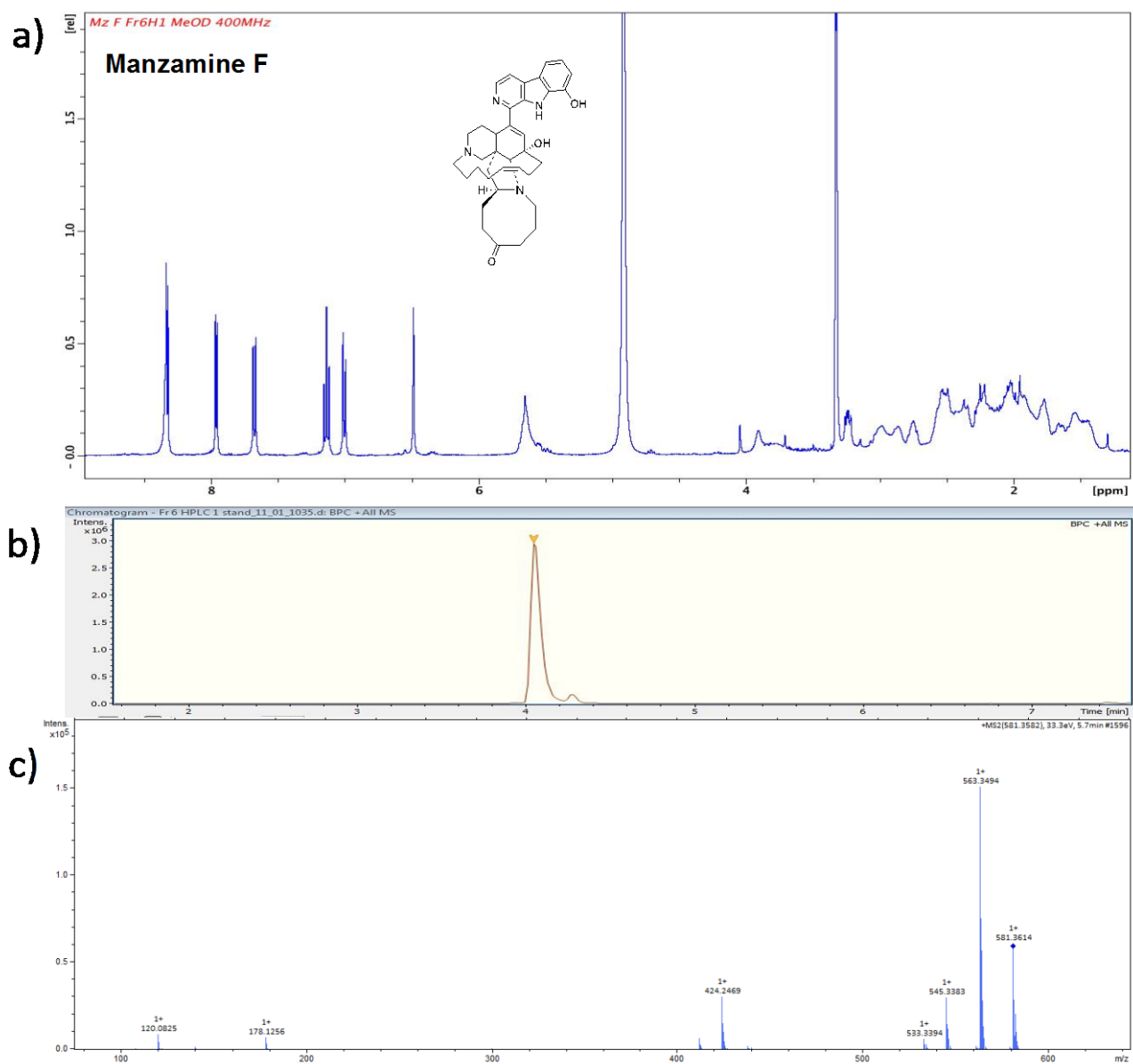
Figure S4. a) ^{1}H NMR spectrum (400 MHz, Methanol-d4), b) LCMS and c) MS/MS of manzamine F (**4**).

a) Fr 6 HPLC 4 MeOD 400Mz

Manzamine X

b) BPC +All MS

c) +MS2(581.3592), 33.3eV, 7.2min #2025
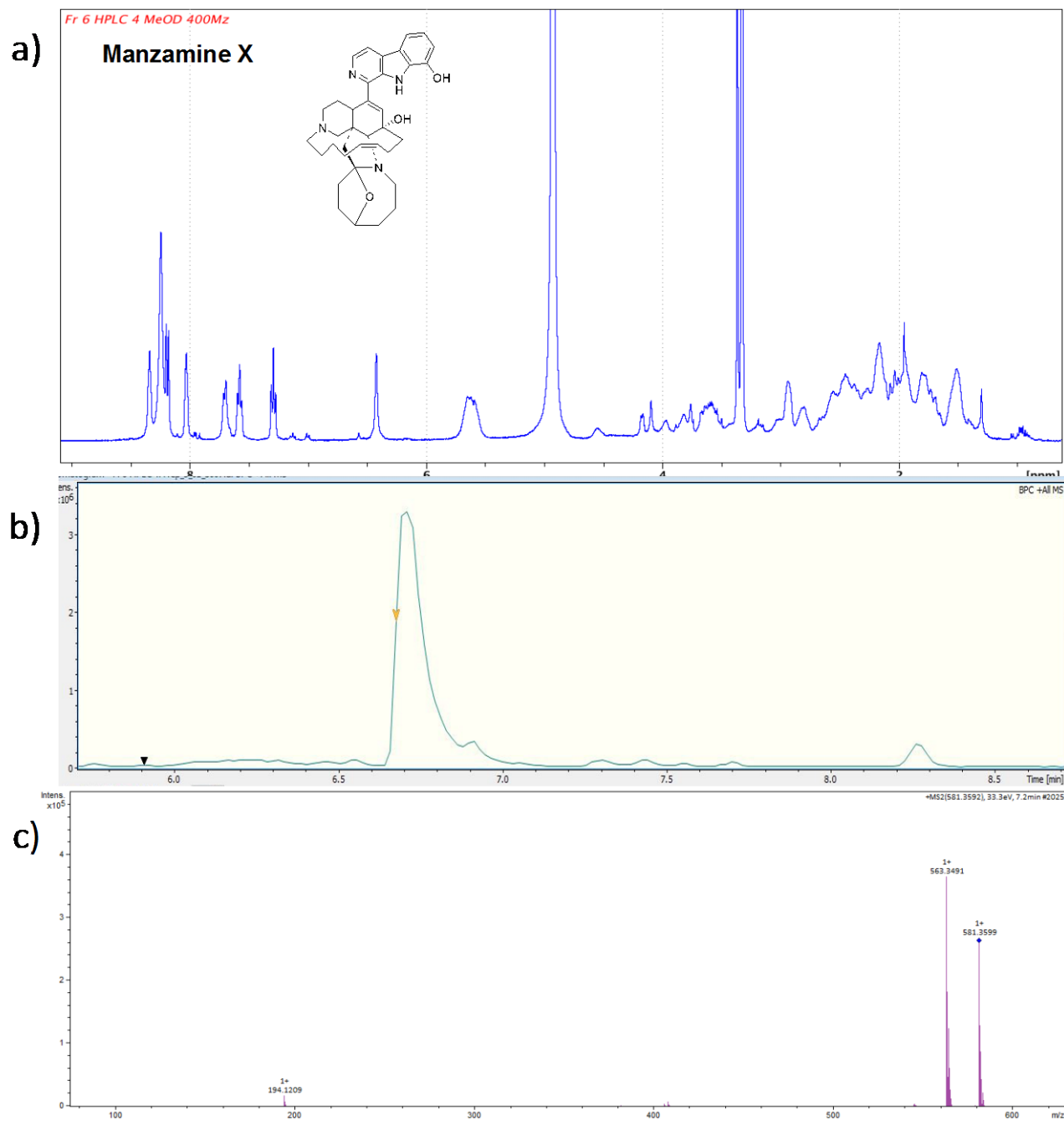
Figure S5. a) ¹H NMR spectrum (400 MHz, Methanol-d4), b) LCMS and c) MS/MS of manzamine X (**5**).

a) **6-cyclohexamidomanzamine A**

b) 11_51_01_8193.d: TIC +All MS

c) +MS, 9.9-10.3min #(794-827)
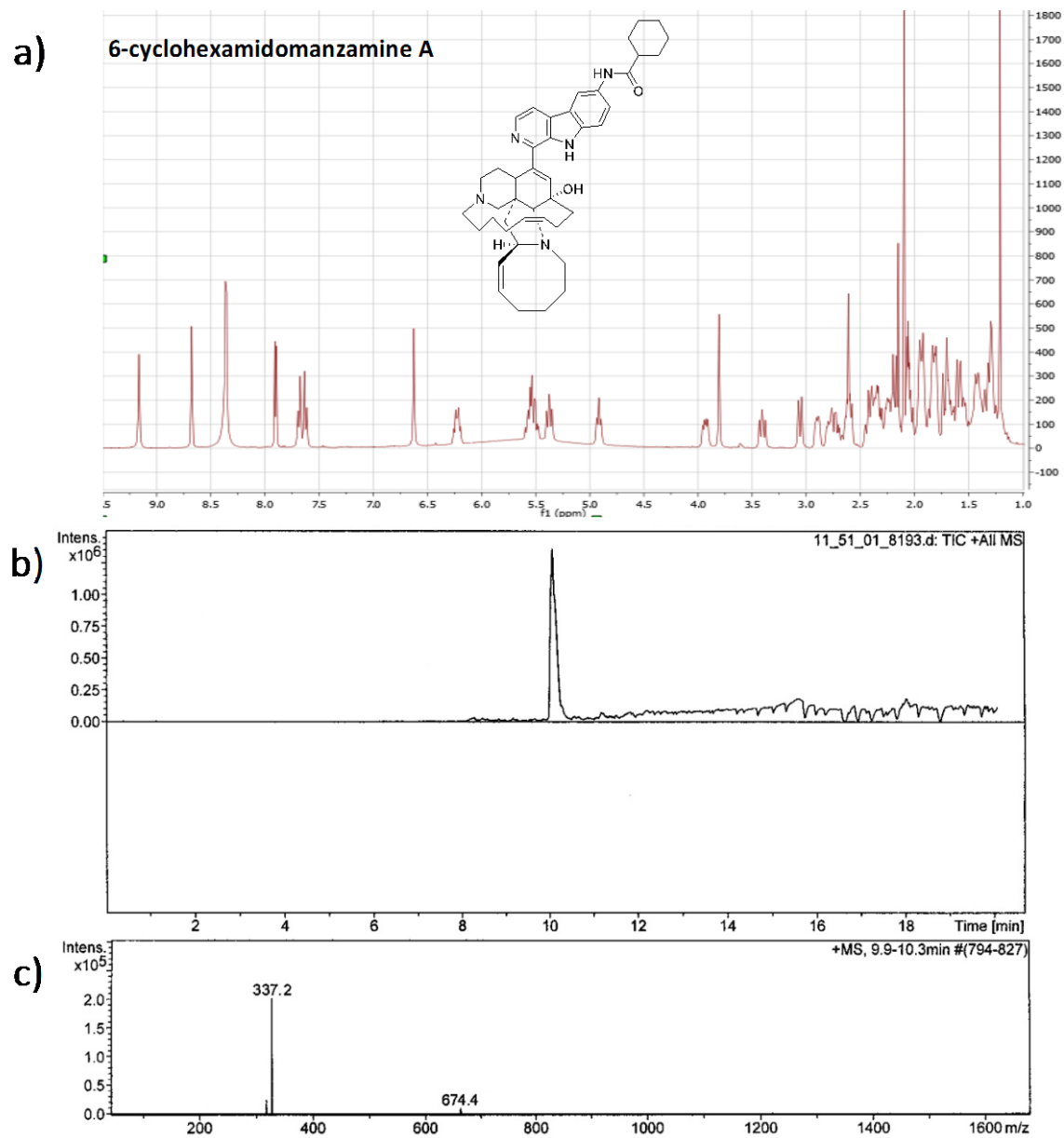
Figure S6. a) ¹H NMR spectrum (400 MHz, Methanol-d4+drops of Acetone), b) LCMS and c) LRMS of 6-cyclohexamidomanzamine A (**6**).

Analyses of Rapid Reversible Inhibition: Equations and Data

Shikimate kinase catalyzes a phosphoryl transfer from ATP to shikimate (SA) in order to form ADP and shikimate-3-phosphate (S3P). Consistent with a wealth of structural data including free MtSK and its complexes with substrates and/or substrate analogs, kinetic evaluation indicates that the enzyme follows a random-sequential substrate binding model.[1] Stated another way, all indications are that the term "α" (see Fig. 2) is close to 1.[1] To determine the possible participation of common rapid-reversible modes of inhibition (i.e., competitive vs uncompetitive vs pure noncompetitive vs mixed noncompetitive), we evaluated our kinetic data in the context of a cuboid model (see Fig. 2).[2] Such a model allows that the inhibitor (I) is capable of binding the free enzyme (E), either ES binary complex (i.e, E-SA and E-ATP), and the ternary E-SA-ATP complex. Using rapid-equilibrium assumptions, a rate equation can be derived to approximate MtSK kinetic behavior in the presence of such a rapid-reversible inhibitor (equation S1). Here, the influence

$$v_o/[\text{E}]_\text{T} = \frac{k_{cat}[\text{SA}][\text{ATP}]}{\alpha K_{ATP}K_{SA} + \alpha K_{ATP}[\text{SA}] + \alpha K_{SA}[\text{ATP}] + \alpha K_{ATP}K_{SA}[\text{I}]/K_I + [\text{SA}][\text{ATP}] + \alpha K_{ATP}[\text{SA}][\text{I}]/\gamma K_I + \alpha K_{SA}[\text{ATP}][\text{I}]/\beta K_I + [\text{SA}][\text{ATP}][\text{I}]/\beta\gamma K_I}$$

of ATP and inhibitor (I) on one another's binding is accounted for by the term "β", and the influence of shikimate (SA) and (I) on one another's binding is accounted for by the term "γ". As such, four K_I terms are anticipated, K_I for I binding to the free enzyme, βK_I to describe I binding to the E-ATP complex, γK_I to describe I binding to the E-SA, and $\beta\gamma K_I$ to describe I binding to the ternary complex. Of course, equation S1 can be divided into two. Equation S2 applies when the concentration of ATP is held constant and SA is varied, and equation S3 applies when the concentration of SA is held constant and ATP is varied. Further,

$$\frac{v_o}{[\text{E}]_\text{T}} = \frac{k_{cat}[\text{SA}]}{\alpha K_{SA}\left(1 + \frac{K_{ATP}}{[\text{ATP}]} + \frac{K_{ATP}[\text{I}]}{[\text{ATP}]K_I} + \frac{[\text{I}]}{\beta K_I}\right) + [\text{SA}]\left(1 + \frac{\alpha K_{ATP}}{[\text{ATP}]} + \frac{\alpha K_{ATP}[\text{I}]}{[\text{ATP}]\gamma K_I} + \frac{[\text{I}]}{\beta\gamma K_I}\right)} \quad \textbf{(S2)}$$

$$\frac{v_o}{[\text{E}]_\text{T}} = \frac{k_{cat}[\text{ATP}]}{\alpha K_{ATP}\left(1 + \frac{K_{SA}}{[\text{SA}]} + \frac{K_{SA}[\text{I}]}{[\text{SA}]K_I} + \frac{[\text{I}]}{\gamma K_I}\right) + [\text{ATP}]\left(1 + \frac{\alpha K_{SA}}{[\text{SA}]} + \frac{\alpha K_{SA}[\text{I}]}{[\text{SA}]\beta K_I} + \frac{[\text{I}]}{\beta\gamma K_I}\right)} \quad \textbf{(S3)}$$

under circumstances where the concentration of the constant substrate is saturating (i.e., [ATP]$>>K_{ATP}$ and αK_{ATP} or [SA]$>>K_{SA}$ and αK_{SA}), then equations 2 and 3 can be approximated by equations S4 and S5, respectively.[2] Each of these equations would support a mixed-inhibition model.

$$\frac{v_o}{[\text{E}]_\text{T}} = \frac{k_{cat}[\text{SA}]}{\alpha K_{SA}\left(1 + \frac{[\text{I}]}{\beta K_I}\right) + [\text{SA}]\left(1 + \frac{[\text{I}]}{\beta\gamma K_I}\right)} \quad \textbf{(S4)}$$

$$\frac{v_o}{[\text{E}]_\text{T}} = \frac{k_{cat}[\text{ATP}]}{\alpha K_{ATP}\left(1 + \frac{[\text{I}]}{\gamma K_I}\right) + [\text{ATP}]\left(1 + \frac{[\text{I}]}{\beta\gamma K_I}\right)} \quad \textbf{(S5)}$$

Using the Prism software mixed inhibition model, two inhibition parameters are returned, "α" and "K_I". Translating to the two-substrate system of MtSK, "α" would correspond to γ and "K_I" would correspond to βK_I in experiments where ATP was held at constant and saturating concentrations. Likewise, "α" would correspond to β, and "K_I" would correspond to γK_I in experiments where SA was held at constant

and saturating concentrations. This approach for evaluating MtSK inhibition by manzamine A (**1**) is shown for experiments where SA was held constant and ATP varied (Fig. S7A) and for experiments where ATP was held constant and SA varied (Fig. S7D). The same type of analysis for MtSK inhibition by 6-cyclohexamidomanzamine A (**6**) is shown for constant SA (Fig. S8A) and constant ATP (Fig. S8D).

An alternative way to evaluate these kinetic data is to determine the effect of inhibitor on the apparent k_{cat} of MtSK as well as the apparent k_{on} (i.e., k_{cat}/K_M) with respect to each substrate. This involves fitting reach curve to determine its individual Michaelis-Menten parameters (k_{on} or k_{cat}/K_M). The individually fit rate curves for each concentration of manzamine A (**1**) can be found in Fig. S7B (constant shikimate; varied ATP) and Fig. S7E (constant ATP; varied shikimate). The same can be found for cyclohexamidomanzamine A (6) in Fig. S8B and S8E, respectively. From equation S2 (experiments carried out with constant concentrations of ATP), the apparent $k_{on[SA]}$ (i.e., k_{cat}/K_M with respect to SA) is given by equation S6, and the apparent k_{cat} is given by equation S7. In a similar manner,

$$\left(k_{on[SA]}\right)_{app} = \frac{k_{cat}}{\alpha K_{SA}\left(1 + \frac{K_{ATP}}{[ATP]} + \frac{K_{ATP}[I]}{[ATP]K_I} + \frac{[I]}{\beta K_I}\right)} \quad \textbf{(S6)}$$

$$(\textbf{S7}) \quad (k_{cat})_{app} = \frac{k_{cat}}{\left(1 + \frac{\alpha K_{ATP}}{[ATP]} + \frac{\alpha K_{ATP}[I]}{[ATP]\gamma K_I} + \frac{[I]}{\beta\gamma K_I}\right)} \quad \textbf{(S7)}$$

when SA is held constant the apparent $k_{on[ATP]}$ (i.e., the apparent k_{cat}/K_M with respect to ATP) is given by equation S8, and the apparent k_{cat} is given by equation S9. Supposing that the fixed-concentration

$$\left(k_{on[ATP]}\right)_{app} = \frac{k_{cat}}{\alpha K_{ATP}\left(1 + \frac{K_{SA}}{[SA]} + \frac{K_{SA}[I]}{[SA]K_I} + \frac{[I]}{\gamma K_I}\right)} \quad \textbf{(S8)}$$

$$(k_{cat})_{app} = \frac{k_{cat}}{\left(1 + \frac{\alpha K_{SA}}{[SA]} + \frac{\alpha K_{SA}[I]}{[SA]\beta K_I} + \frac{[I]}{\beta\gamma K_I}\right)} \quad \textbf{(S9)}$$

substrate is at a saturating concentration, equations S6 – S9 simplify to three equations. When ATP is the fixed substrate, the effect of inhibitor on the apparent k_{cat}/K_M with respect to SA (i.e., $k_{on(SA)}$) (equation S10) can be used to estimate βK_I. When SA is the fixed substrate, the effect of inhibitor on the apparent k_{cat}/K_M with respect to ATP (i.e., $k_{on(ATP)}$) (equation S11) can be used to estimate γK_I.

$$\left(k_{on[SA]}\right)_{app} = \frac{k_{cat}}{\alpha K_{SA}\left(1 + \frac{[I]}{\beta K_I}\right)} \quad \textbf{(S10)}$$

$$\left(k_{on[ATP]}\right)_{app} = \frac{k_{cat}}{\alpha K_{ATP}\left(1 + \frac{[I]}{\gamma K_I}\right)} \quad \textbf{(S11)}$$

Finally, $\beta\gamma K_I$ can be determined when either ATP or SA is the fixed substrate at saturating concentration, because the effect of inhibitor on the apparent k_{cat} (equation S12) is the same in either case.

$$(k_{cat})_{app} = \frac{k_{cat}}{\left(1 + \frac{[I]}{\beta\gamma K_I}\right)} \qquad (\textbf{S12})$$

The applications of equations S12 and S11 to evaluate inhibition of *Mt*SK by **1** with fixed saturating SA and varied ATP are shown in Figs. S7C and S7D, respectively. The applications of equations S12 and S10 to evaluate inhibition of *Mt*SK by **1** with fixed saturating ATP and varied SA are shown if Fig. S7G and S7H, respectively. Likewise, the applications of equations S12 and S11 to evaluate inhibition of *Mt*SK by **6** with fixed saturating SA and varied ATP are shown in Figs. S8C and S8D, respectively. The applications of equations S12 and S10 to evaluate inhibition of *Mt*SK by **6** with fixed saturating ATP and varied SA are shown if Figs. S8G and S8H, respectively. The analogous experiments for 6-hydroxymanzamine A (**2**), manzamine E (**3**), manzamine F (**4**), and 6-deoxymanzamine X (**5**) are presented in Figs. S9, S10, S11, and S12, respectively. In all replots, the error bars show the standard errors from the fit of the individual rate curves to equation 1.

Given the observation of time-dependent inhibition with these compounds, it is important to ascertain the extent to which the analyses of the standard steady-state inhibition experiments (see above) may be distorted by the increase in inhibition over time. We used kinetic modeling to determine the expected impact of time-dependent inhibition on steady-state inhibition assays carried out as described. Our model was based on the inhibitor with the largest k_5 and the largest k_5/k_6 ratio (i.e., **6**), and therefore, the inhibitor likely to produce the greatest distortion in steady-state inhibition studies. Whether the *Mt*SK mechanism was represented as a simple single-substrate, single-product Michaelis-Menten enzyme, or more accurately as a random sequential bi-bi enzyme, the results were nearly identical; the largest impact of time-dependent inhibition was observed when the inhibitor was able to bind to all enzyme-substrate complexes and the slow isomerization step could occur from any initial enzyme inhibitor complex. Even under a model to maximize the effect, time-dependent inhibition was predicted to have very little impact on *Mt*SK activity within the 30-s time window of our steady-state enzyme assays (Fig. S13).
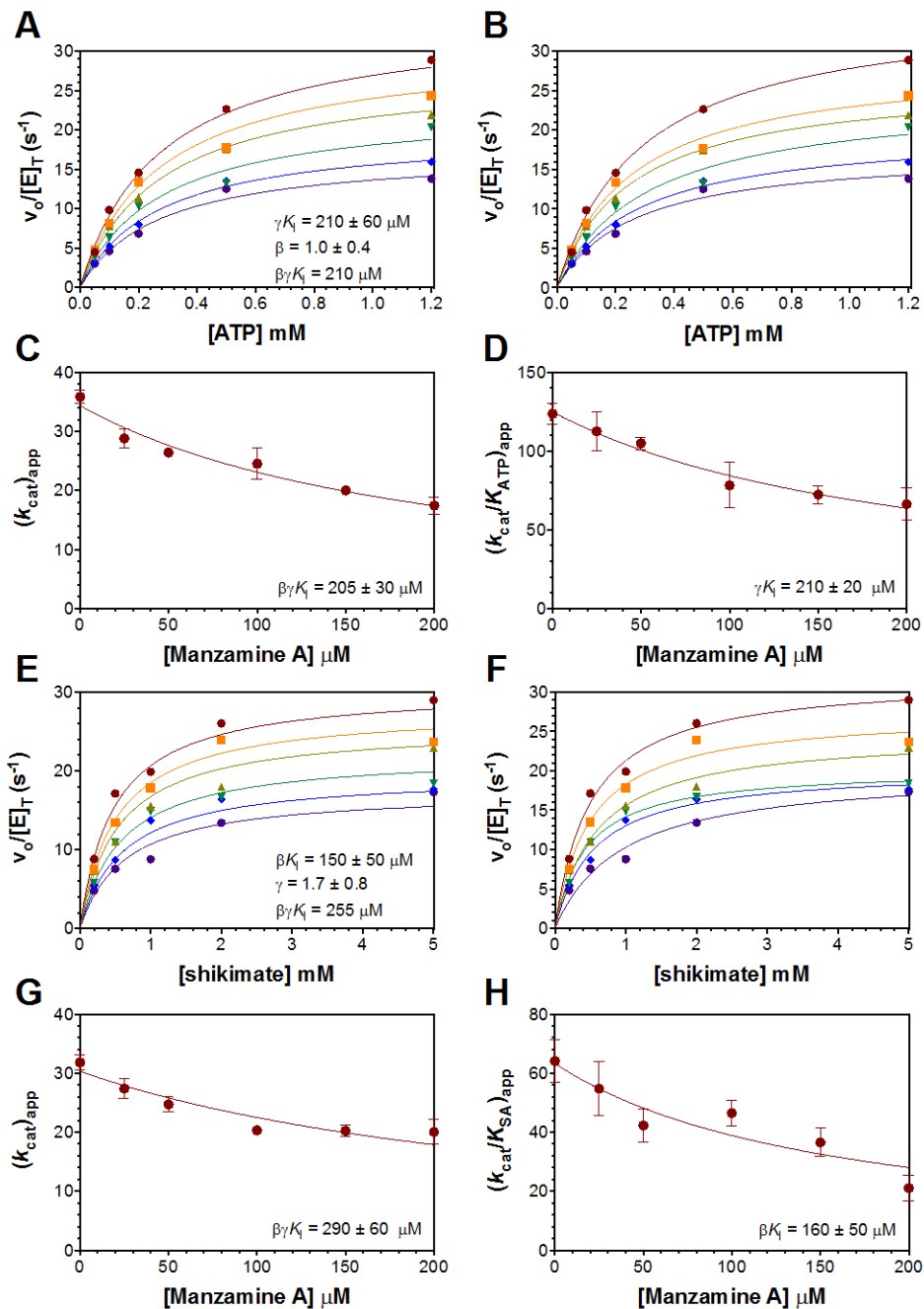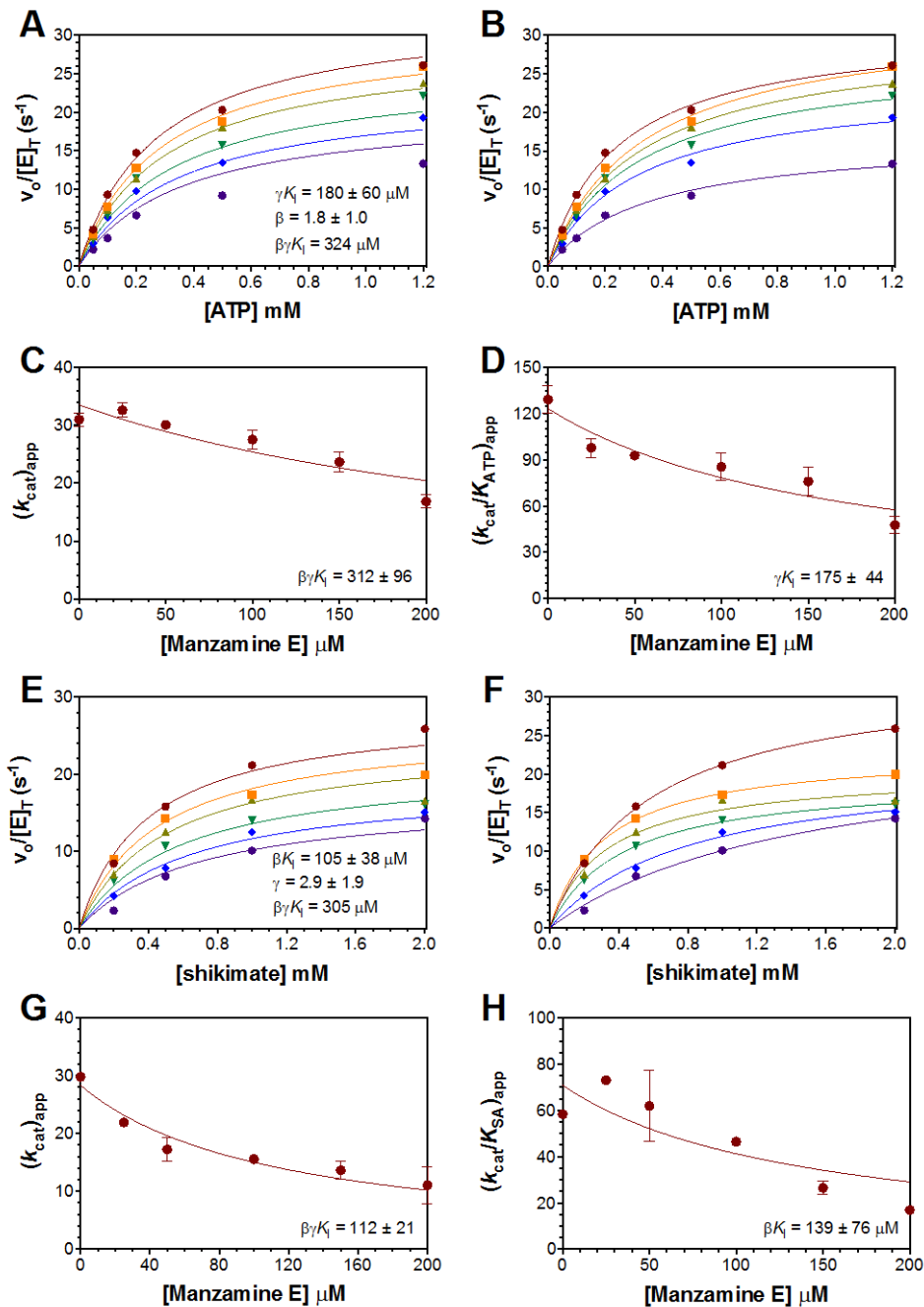
Figure S7. Non-linear least-squares analyses of rapid reversible inhibition by manzamine A (1). Data acquired varying [ATP] at fixed [SA] were either fit to a global mixed-noncompetitive mechanism of inhibition (A) or as individual Michaelis-Menten curves (B). Replots of $(k_{cat})_{app}$ and $(k_{cat}/K_M)_{app}$ obtained from panel B as a function of **1** are shown in (C) and (D), respectively. Data acquired varying [SA] at fixed [ATP] were either fit to a global mixed-noncompetitive mechanism of inhibition (E) or as individual Michaelis-Menten curves (F). Replots of $(k_{cat})_{app}$ and $(k_{cat}/K_M)_{app}$ obtained from panel F as a function of **1** are shown in (G) and (H), respectively. Concentrations of **1** evaluated were 0 (●), 25 (■), 50 (▲), 100 (▼), 150 (◆), and 200 (●) μM.
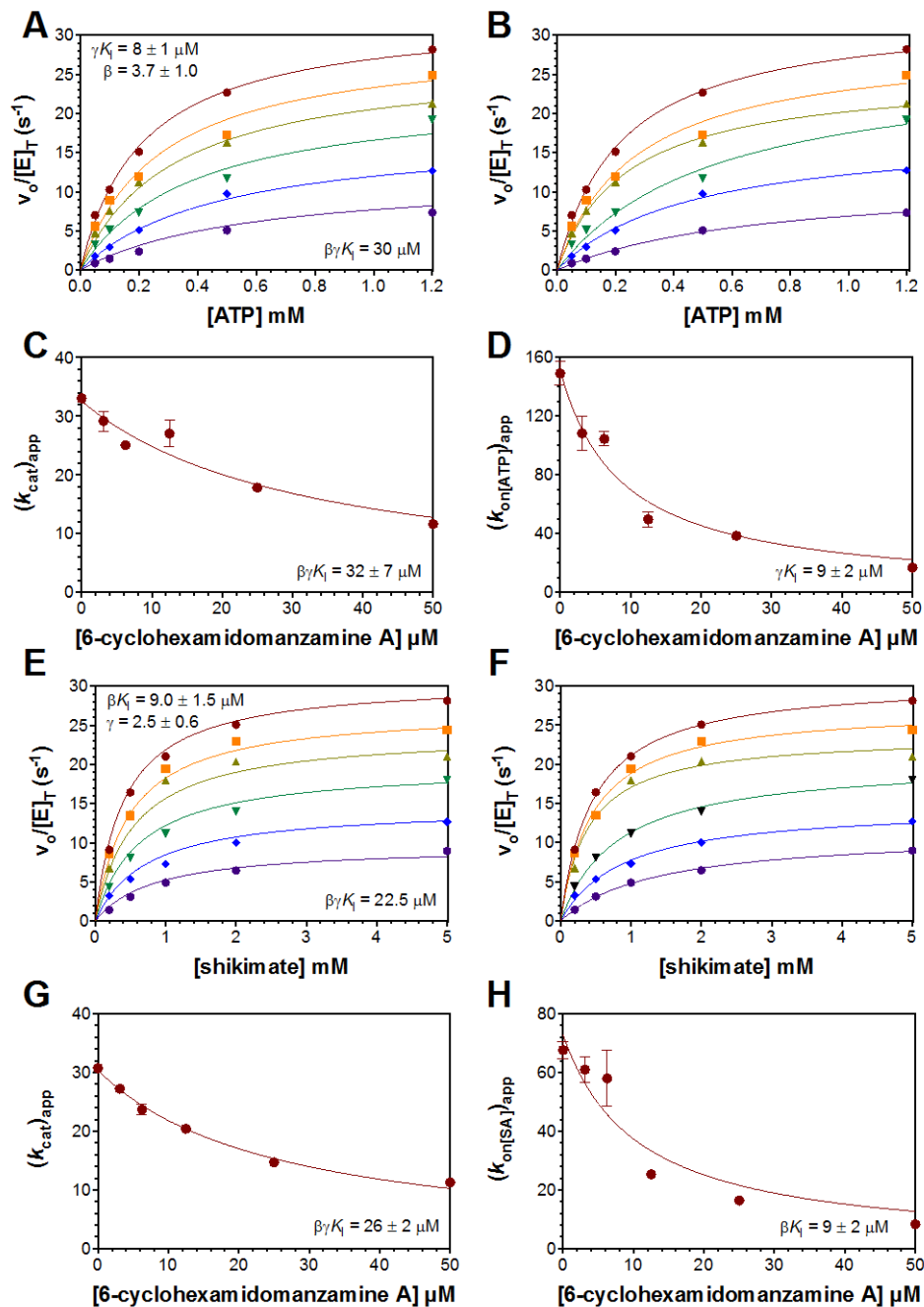
Figure S8. Non-linear least-squares analyses of rapid reversible inhibition by 6-cyclohexamido-manzamine A (6). Data acquired varying [ATP] at fixed [SA] were either fit to a global mixed-noncompetitive mechanism of inhibition (A) or as individual Michaelis-Menten curves (B). Replots of $(k_{cat})_{app}$ and $(k_{cat}/K_M)_{app}$ obtained from panel B as a function of **6** are shown in (C) and (D), respectively. Data acquired varying [SA] at fixed [ATP] were either fit to a global mixed-noncompetitive mechanism of inhibition (E) or as individual Michaelis-Menten curves (F). Replots of $(k_{cat})_{app}$ and $(k_{cat}/K_M)_{app}$ obtained from panel F as a function of **6** are shown in (G) and (H), respectively. Concentrations of **6** evaluated were 0 (●), 3.12 (■), 6.25 (▲), 12.5 (▼), 25 (◆), and 50 (●) μM.
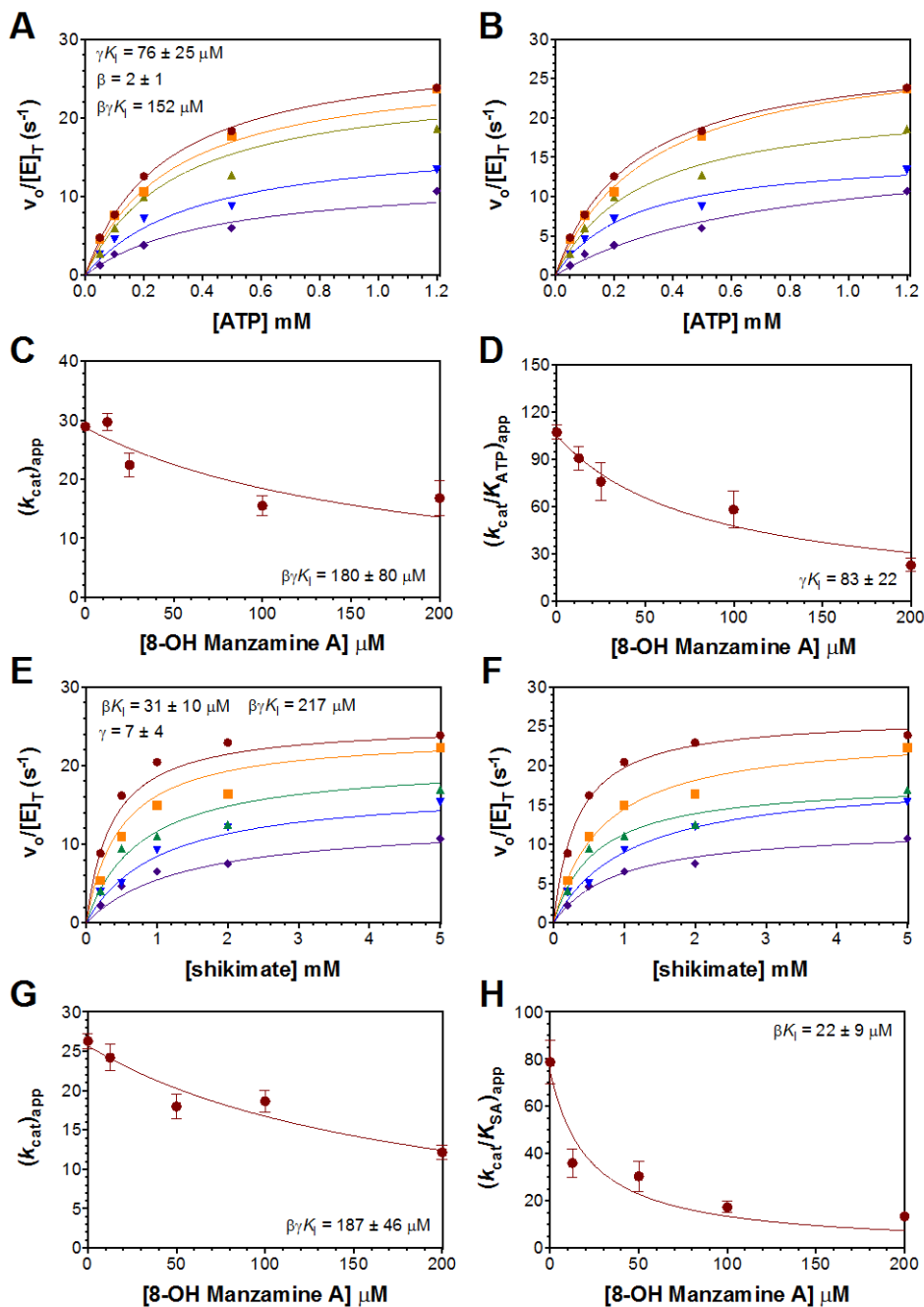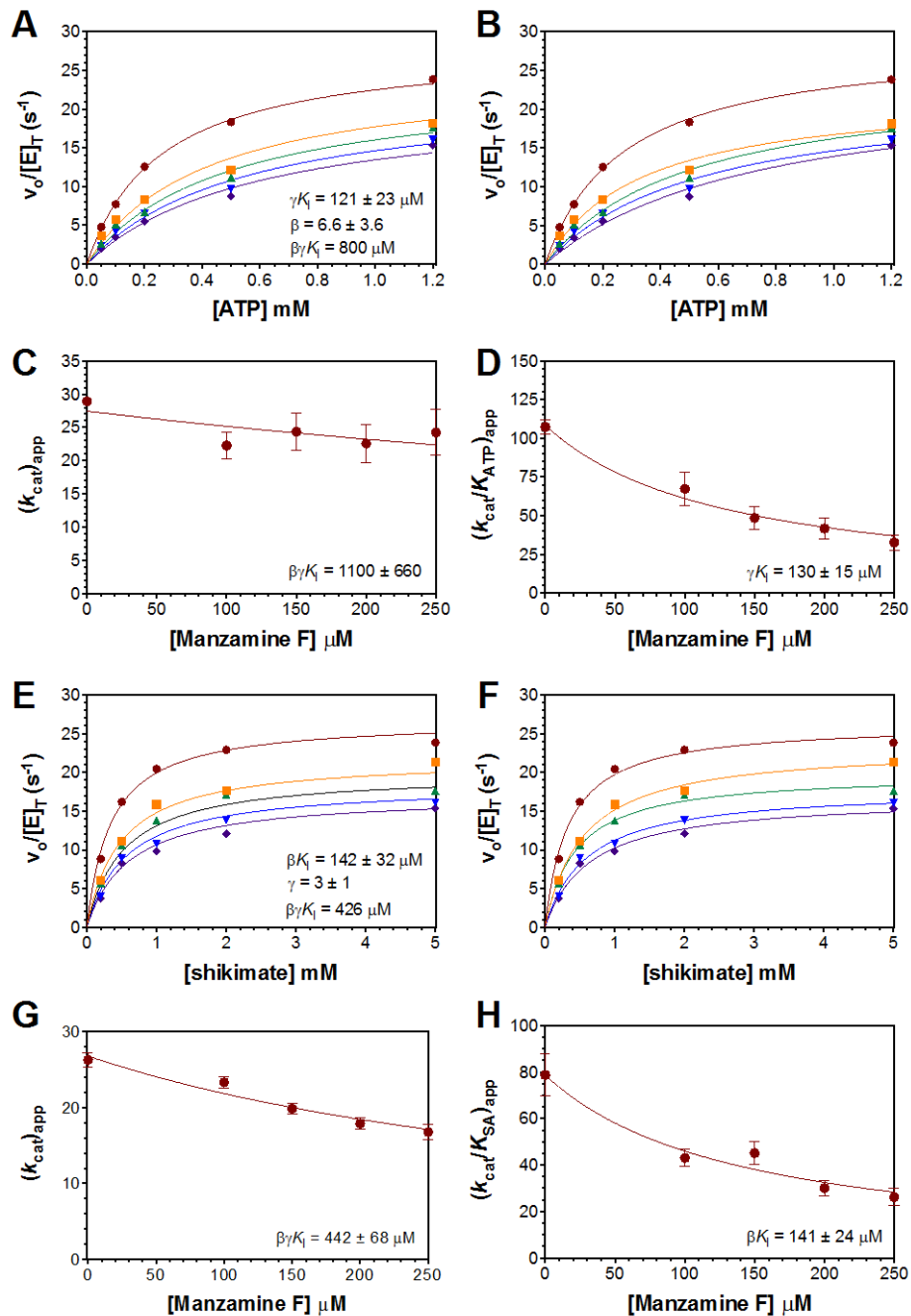
Figure S9. Non-linear least-squares analyses of rapid reversible inhibition by 8-hydroxymanzamine A (2). Data acquired varying [ATP] at fixed [SA] were either fit to a global mixed-noncompetitive mechanism of inhibition (A) or as individual Michaelis-Menten curves (B). Replots of $(k_{cat})_{app}$ and $(k_{cat}/K_M)_{app}$ obtained from panel B as a function of **2** are shown in (C) and (D), respectively. Data acquired varying [SA] at fixed [ATP] were either fit to a global mixed-noncompetitive mechanism of inhibition (E) or as individual Michaelis-Menten curves (F). Replots of $(k_{cat})_{app}$ and $(k_{cat}/K_M)_{app}$ obtained from panel F as a function of **2** are shown in (G) and (H), respectively. Concentrations of **2** evaluated were 0 (●), 12.5 (■), 25 (▲)/50 (▲), 100 (▼), and 200 (◆) μM.

Figure S10. Non-linear least-squares analyses of rapid reversible inhibition by manzamine E (3). Data acquired varying [ATP] at fixed [SA] were either fit to a global mixed-noncompetitive mechanism of inhibition (A) or as individual Michaelis-Menten curves (B). Replots of $(k_{cat})_{app}$ and $(k_{cat}/K_M)_{app}$ obtained from panel B as a function of **3** are shown in (C) and (D), respectively. Data acquired varying [SA] at fixed [ATP] were either fit to a global mixed-noncompetitive mechanism of inhibition (E) or as individual Michaelis-Menten curves (F). Replots of $(k_{cat})_{app}$ and $(k_{cat}/K_M)_{app}$ obtained from panel F as a function of **3** are shown in (G) and (H), respectively. Concentrations of **3** evaluated were 0 (●), 25 (■), 50 (▲), 100 (▼), 150 (◆), and 200 (●) μM.
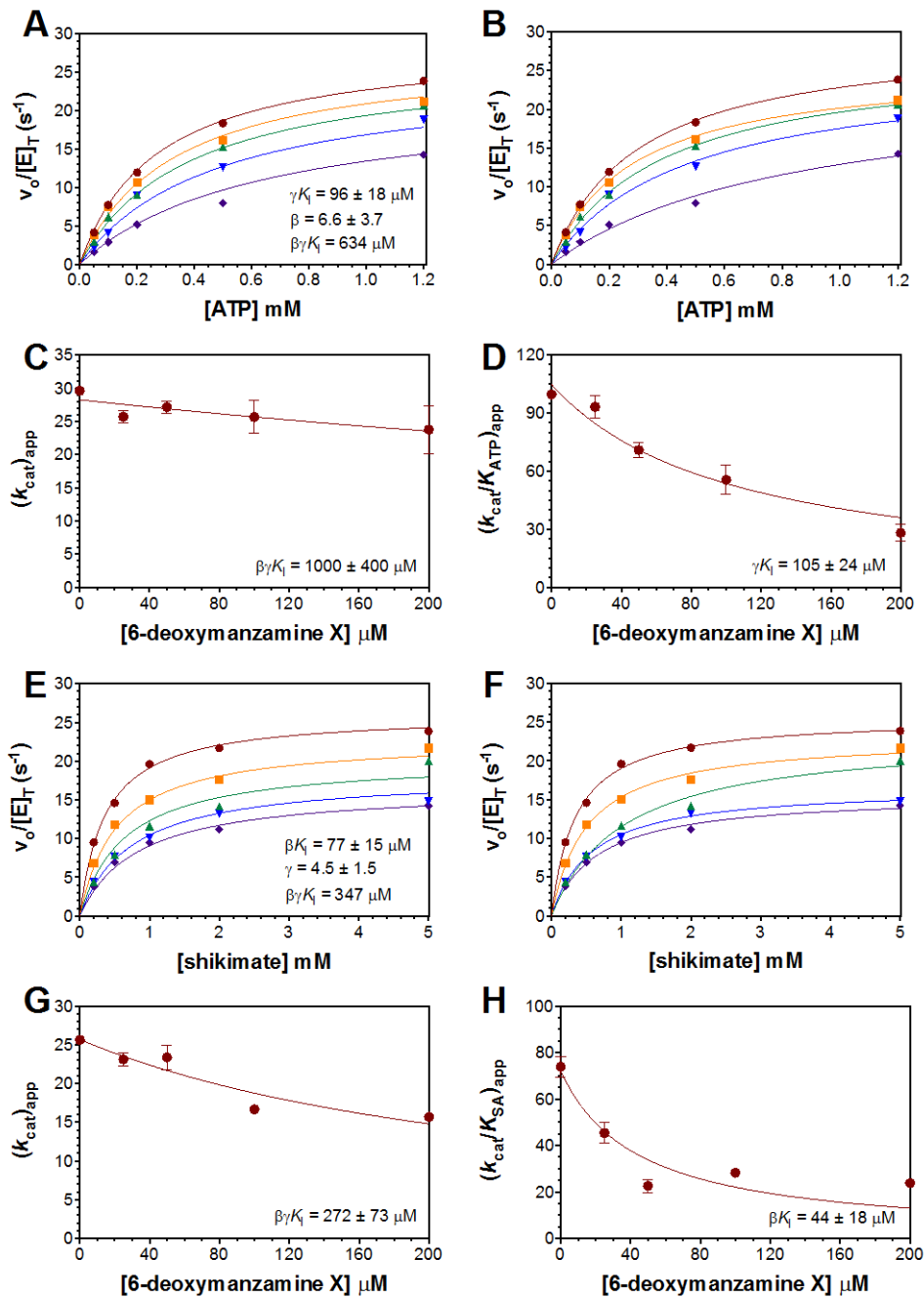
Figure S11. Non-linear least-squares analyses of rapid reversible inhibition by manzamine F (4). Data acquired varying [ATP] at fixed [SA] were either fit to a global mixed-noncompetitive mechanism of inhibition (A) or as individual Michaelis-Menten curves (B). Replots of $(k_{cat})_{app}$ and $(k_{cat}/K_M)_{app}$ obtained from panel B as a function of **4** are shown in (C) and (D), respectively. Data acquired varying [SA] at fixed [ATP] were either fit to a global mixed-noncompetitive mechanism of inhibition (E) or as individual Michaelis-Menten curves (F). Replots of $(k_{cat})_{app}$ and $(k_{cat}/K_M)_{app}$ obtained from panel F as a function of **4** are shown in (G) and (H), respectively. Concentrations of **4** evaluated were 0 (●), 100 (■), 150 (▲), 200 (▼), and 250 (◆) μM.

Figure S12. Non-linear least-squares analyses of rapid reversible inhibition by deoxymanzamine X (5). Data acquired varying [ATP] at fixed [SA] were either fit to a global mixed-noncompetitive mechanism of inhibition (A) or as individual Michaelis-Menten curves (B). Replots of $(k_{cat})_{app}$ and $(k_{cat}/K_M)_{app}$ obtained from panel B as a function of **5** are shown in (C) and (D), respectively. Data acquired varying [SA] at fixed [ATP] were either fit to a global mixed-noncompetitive mechanism of inhibition (E) or as individual Michaelis-Menten curves (F). Replots of $(k_{cat})_{app}$ and $(k_{cat}/K_M)_{app}$ obtained from panel F as a function of **5** are shown in (G) and (H), respectively. Concentrations of **5** evaluated were 0 (●), 25 (■), 50 (▲), 100 (▼), and 200 (◆) μM.
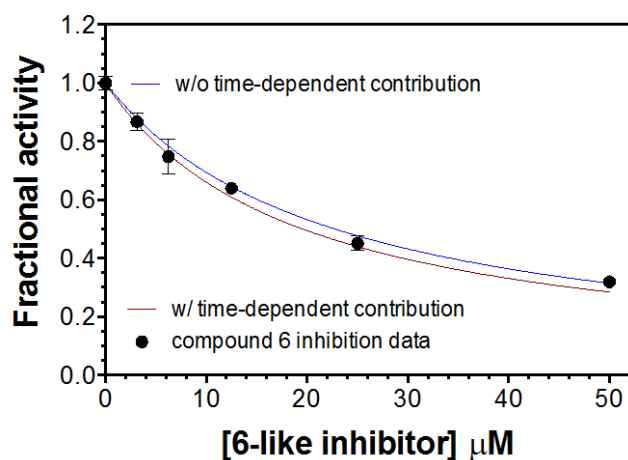
Figure S13. Modeled effect of an inhibitor with compound 6 parameters on the activity of an *Mt*SK-like enzyme in steady-state inhibition assays. The model was constructed according to Fig. 2. For the inhibitor, the initial encounter K_D's were modeled after K_I's from Tables 1 and 2: 2 μM (free E), 8 μM (each binary complex E-ATP and E-SA), and 32 μM (ternary E-ATP-SA complex). To observe the maximum possible interference of time-dependent inhibition, the slow transition to EI* complexes was presumed to be possible from any enzyme inhibitor complex. The red line corresponds to modeled activity where k_5 is 0.015 s^{-1} (i.e., 0.91 min^{-1}) and k_6 is 0.00067 s^{-1} (i.e., 0.04 min^{-1}; see Table 3). The blue line corresponds to modeled activity where $k_5 = 0$ (i.e., there is no time-dependent inhibition). Activity is modeled with 5 mM SA and 1.2 mM ATP. For reference, actual inhibition data obtained with compound **6** under identical conditions are shown.

Kinetic modeling for jump-dilution experiments

The recoveries of MtSK activity following jump-dilution of preformed manzamine-MtSK complexes were broadly consistent with the superior properties of **6** as an inhibitor (i.e., low K_I's, high k_5, and low k_6) relative to **1** – **5**. However, the post-dilution acceleration of activity typical of reversible, slow-onset inhibitors was not observed for **1** – **5** (see Fig. 6). To evaluate the set up of our jump-dilution experiments as well as garner some insight into this apparent inconsistency, we used KinTek Explorer software construct simplified kinetic models and evaluate broad features of anticipated results.[3] It should be emphasized that these are not intended to be global analyses of comprehensive kinetic models. As yet, there are still many unknowns that preclude the effective application of such methods.

Based on a two-step model for formation of an EI* complex (Fig. S14B) as well as values for K_I (Table 1), k_5, and k_6 (Table 3) we evaluated the extent to which an EI* complex would be expected to accumulate during a one-hour preincubation between 20 µM MtSK and 1 mM inhibitor. As shown for **1** (Fig. S14A) and calculated for **2**, **3**, and **6**, rapid-equilibrium formation of EI is followed by the k_5/k_6-dominated transition to EI* over the course or preincubation such that in each case the dominant species at the conclusion of preincubation was anticipated to be EI* (Table S2). Supposing a simplified enzyme mechanism (i.e., one S, one ES complex) including mixed noncompetitive inhibition and the conversion of EI to EI* (Fig. S15A), we estimated the change in distribution of enzyme states following 1:100 dilution into a reaction containing a saturating concentration of substrate. For **1** (Fig. S15B) as well as **2**, **3**, and **6** (Table S3), we supposed the rapid-equilibrium conversion of EI to E, essentially, at the time of dilution. Over the course of the assay, active enzyme species would then be expected to accumulate at the expense of EI*. Using the fraction of active enzyme species as a basis for estimation, an increase in activity ranging from 2.7 to 5.4 fold was calculated (Table S3). Of course, an increase in activity following dilution was not observed for **1** – **5** (see Fig. 6). We explored the possibility that product accumulation may interfere with an expected acceleration of activity in a jump-dilution experiment like ours. Including the conversion of E + P to ES in the mechanism markedly changed the results one would expect; similar to what we observed with **1** – **5** (Fig. 6), an acceleration of product generation was no longer evident (e.g., with **1**, Fig. S16) and more closely resembled our experimental results (Fig. S16C). Also consistent with our experimental observations, an inhibitor with the properties of **6** would still show a delay in the recovery of activity (Fig. S16D).
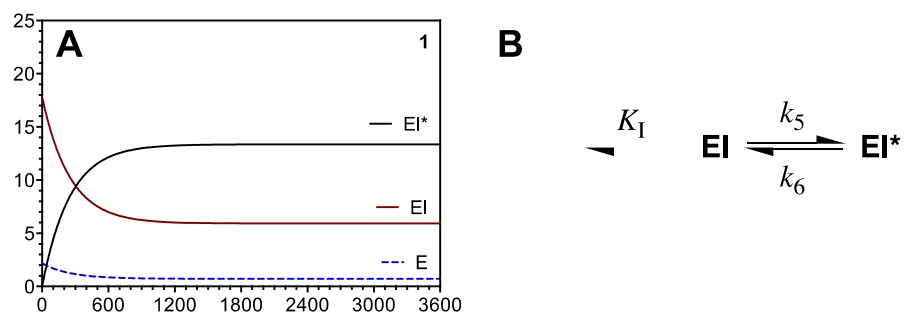
Figure S14. Preincubation association of *Mt*SK with 1 (A) from free enzyme (E) to initial rapid-equilibrium complex (EI) to the slow-onset complex (EI*) (B). The reaction conditions matched those of the preincubation in our jump-dilution experiments (i.e., 20 μM *Mt*SK and 1 mM inhibitor). The parameters were as follows: K_I = 120 μM (Table 1), k_5 = 0.003 s^{-1} (i.e., 0.18 min^{-1}) and k_6 = 0.0013 s^{-1} (i.e., 0.08 min^{-1}) (Table 3).

Table S2. Relative concentrations of enzyme states at the end of preincubation

Inhibitor	Fraction[a]		
	[E]	[EI]	[EI*]
1	0.036	0.296	0.668
2	0.002	0.159	0.839
3	0.008	0.127	0.864
6	< 0.001	0.042	0.958

[a]Fraction of the 20 μM total *Mt*SK in the indicated state following 1 hr preincubation.
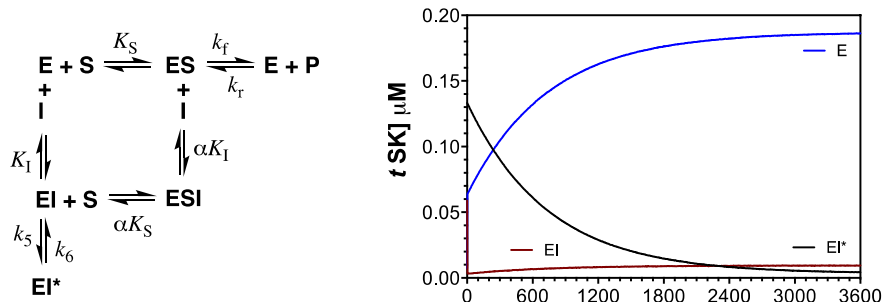
Figure S15. **Predicted post-dilution recovery of *Mt*SK following preincubation with 1.** The enzyme model (A) was simplified to a single substrate, single product, single ES complex system and allowed for mixed noncompetitive inhibition in the rapid equilibrium phase. Following a nearly instantaneous conversion of EI to E upon dilution (compare E at t = 3600 s in the left panel of Figure S14 to E at t = 3.6 s here), slow accumulation of E is observed consistent with the loss of EI*. Consistent with the post-dilution conditions of our jump-dilution experiments, the sum of all *Mt*SK species is 0.2 μM. E represents all active forms of enzyme (E and ES), and EI represents the sum of EI and ESI complexes. Parameters/constants were as follows: K_S = 0.5 mM, K_I = 0.120 mM (from Table 1), α = 1.75 (γK_I/K_I from Table 1), k_5 = 0.003 s^{-1} (0.18 min^{-1} from Table 3), k_6 = 0.0015 s^{-1} (0.08 min^{-1} from Table 3), k_f = 16.7 s^{-1}, and k_r = 0.6 s^{-1}.

Table S3. Calculated activity recovery following dilution.

Inhibitor	Fraction[a] of Active Enzyme		
	Initial[b]	Final[c]	Fold Increase
1	0.35	0.94	2.7
2	0.14	0.60	4.3
3	0.13	0.55	4.2
6	0.019	0.11	5.8

[a]Fraction of the 0.2 μM total *Mt*SK not bound to I (e.g., E, ES, etc.)
[b]Immediately (i.e., 3.6 s) following dilution
[c]1 hour following dilution (i.e., at the conclusion of the assay)
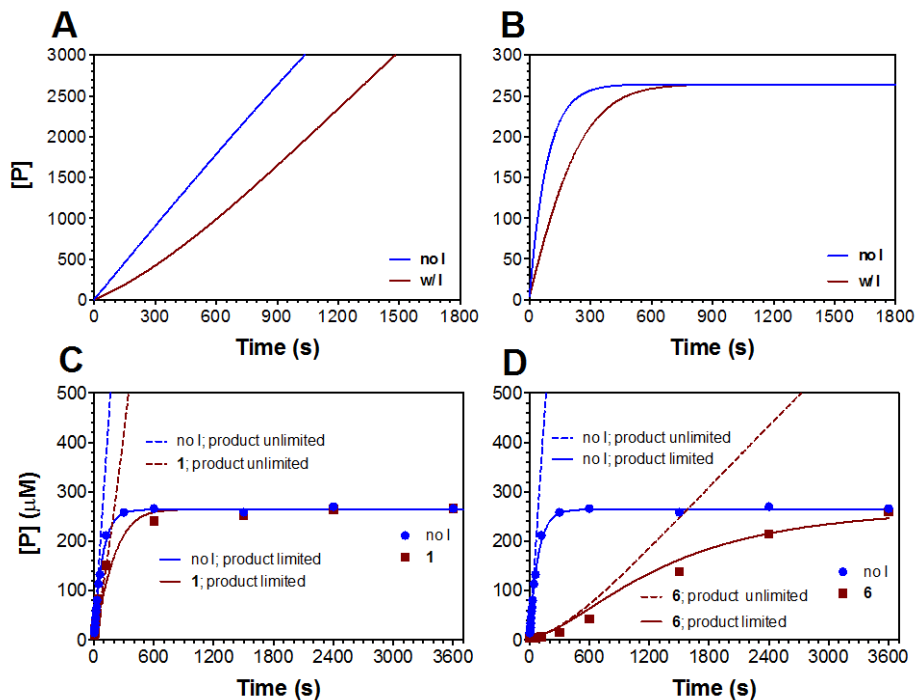
Figure S16. Anticipated activity recovery in a jump-dilution experiment where there is no product interference or product contributes to a back reaction. For panels A and B, inhibitor parameters, preincubation conditions, and dilution conditions were modeled after **1** (identical to Fig. S15). For panel A, k_r = 0, and for panel B, k_r = 0.6 s^{-1}. Modeled versus observed activity recovery in jump-dilution experiments for manzamine A (**1**) (C) and cyclohexamidomanzamine A (**6**) (D). Parameters for modeling activity recovery for **1** and **6** were identical to Fig. S15, except that for **6**, K_I = 3.2 μM, α = 2.5, k_5 = 0.0158 s^{-1}, and k_6 = 0.00033 s^{-1}.

References

(1) Rosado, L. A., Vasconcelos, I. B., Palma, M. S., Frappier, V., Najmanovich, R. J., Santos, D. S., and Basso, L. A. (2013) The Mode of Action of Recombinant Mycobacterium tuberculosis Shikimate Kinase: Kinetics and Thermodynamics Analyses. *PLOS ONE 8*, e61918.

(2) Segel, I. H. (1975) Rapid equilibrium bireactant and terreactant systems, in *Enzyme Kinetics: Behavior and Analysis of Rapid Equilibrium and Steady-State Enzyme Systems, pp 273 – 345*.

(3) Johnson, K. A., Simpson, Z. B., and Blom, T. (2009) Global kinetic explorer: a new computer program for dynamic simulation and fitting of kinetic data. *Anal. Biochem. 387*, 20–29.